International Core Journal of Engineering Volume 11 Issue 7, 2025
ISSN: 2414-1895 DOI: 10.6919/ICJE.202507_11(7).0018

Current Time Optimal Controller for PMSM based on Current Trajectory Planning

Lixiang Sun[1], Haifeng Wei[2], Hanpei Wei[2, a], and Jia Cui[2]

[1] Intelligent agricultural equipment collaborative innovation center of Ministry of Education, Yancheng Polytechnic College, Yancheng 224005, China

[2] School of Automation, Jiangsu University of Science and Technology, Zhenjiang 212003, China

[a]1506089882@qq.com

Abstract

The current time optimal control method is used to plan the voltage command to achieve the shortest current tracking time. By analyzing the time optimal current trajectory, an improved current time optimal control method is proposed. The current transient transition trajectory is optimized by replanning the current command in voltage saturation region. The improved control method not only simplifies the calculation of the algorithm, but also realizes the fast transient-current characteristics in voltage saturation region without affecting the current steady state performance. The experimental results verify the feasibility of the proposed method. Compared with the conventional proportional-integral (PI) current controller, the new current control method maintains the system stability of the motor at high speed and achieves about 27% improvement in current transient response performance.

Keywords

Current Time Optimal Control Method; Current Transient Transition Trajectory; Voltage Saturation Region; PI.

1. Introduction

In recent years, high-end equipment manufacturing is an important field of industrial transformation and upgrading. High performance servo system is one of the focuses, and has been paid more and more attention. Permanent magnet synchronous motor (PMSM) has the advantages of high torque inertia ratio, high power factor and power density. It is widely used in the servo system of automatic manufacturing, intelligent robot, aerospace, ship and other fields. Therefore, the research on high-performance PMSM servo system is of great significance and value to the national economy and national defense construction. The servo system in the above fields often requires wide speed range and small torque ripple, so the PMSM servo system usually adopts vector control. In the three loop control structure based on vector control, the current loop, as the most inner loop, is a key link to affect the performance of PMSM servo system. Therefore, the optimal design of current loop is also one of the research hotspots of high-performance PMSM servo system.

High performance PMSM servo system requires high dynamic response ability of current loop . At present, there are a lot of researches on how to improve the dynamic performance of the current loop, which can be summarized as follows: 1) Modeling the non ideal factors in the motor operation process, and then tuning the controller parameters [1-4]. This method is mainly suitable for specific controlled objects, and its application range is not very wide. 2) Optimizing the current control sequence to shorten the control cycle [5-8]. This method is based on the performance of the hardware, which will

ISSN: 2414-1895 DOI: 10.6919/ICJE.202507_11(7).0018

increase the hardware cost. 3) Adopting the control method based on advanced control theory, which has strong applicability and has no special requirements for hardware. Such as sliding mode variable structure control [9-11], nonlinear PID control [12-14], optimal control [15-17], predictive control [18-20], etc. From the existing research, predictive control is one of the effective and promising control methods. The so-called predictive control means that, based on the mathematical model of the controlled object, the predicted calculated value of the controlled object is compensated to the actual closed-loop feedback, so as to improve the control performance [21,22]. For different applications, many scholars have studied different predictive control algorithms to improve the dynamic performance of the current loop.

In addition to the above research, in view of the requirements of high speed and high dynamic response of permanent magnet synchronous motor, there are still a control problems to be solved in the current inner loop system of PMSM under high speed condition: Under the condition of voltage saturation, the dynamic response performance of current loop system is limited. The details are as follows:

When the bus voltage is not adjustable and the output voltage is not saturated, the output voltage command of the current regulator can be linearly modulated by the inverter, and the actual current will be tracked in real time according to the change of the command. However, when the motor runs at the base speed, the sudden change of current command will make the output voltage command value of the current regulator exceed the limit of voltage limit, and the inverter is in nonlinear modulation state. When the output voltage is saturated, because the voltage output can not be linear output according to the command value, the current control effect will inevitably deteriorate. At present, there are many methods to achieve high dynamic performance of current response under voltage saturation conditions, which can be summarized into the following two categories: 1) The output voltage of the inverter is planned by appropriate over modulation strategy [23-26]. Reference [23] and [24] divide the output voltage command of current controller into two parts: back EMF component and dynamic voltage component. When the voltage is saturated, the back EMF component is kept unchanged and the dynamic voltage component is reprogrammed to minimize the current distortion in the transient process. References [25] and [26] focus on the transient torque action, and propose a voltage command planning scheme to realize the fast response ability of torque. However, the over modulation strategy is based on the current controller output value itself, so the dynamic performance improvement effect of this method has its own limitations. 2) The shortest time of current transient process is realized by current trajectory planning. The most typical application method is the application of time optimal control strategy in current control [27,28]. Under the condition of voltage limitation, the voltage command can be calculated according to the planned time optimal current trajectory. Although this method can achieve the shortest transient transition time, it is difficult in practical application because of its complex calculation and high accuracy requirements. References [29] and [30] proposed a method to modify current instruction based on current error feedback value. In order to achieve the shortest transient process time, the current error term of negative q axis was added in the front end of d axis current input. Although this method can improve the dynamic performance of the current loop, the steady state error deteriorates the stability of the system.

In view of the above problem, this paper is to present a fast transient-current control method for PMSM based on current trajectory replanning in voltage saturation region, which guarantees the system stability of the motor at high speed and improve the output torque response performance in voltage saturation region. The main contributions in this paper is as follows:

The current time optimal control method is used to plan the voltage command to achieve the shortest current tracking time. Considering the computational complexity of the optimal control algorithm, an improved current time optimal control method is proposed by analyzing the time optimal current trajectory. The current transient transition trajectory is optimized by replanning the current command in voltage saturation region. The control method not only simplifies the calculation of the algorithm,

ISSN: 2414-1895 DOI: 10.6919/ICJE.202507_11(7).0018

but also realizes the fast transient-current characteristics in voltage saturation region without affecting the current steady state performance. Different from most flux weakening control methods, the improved current time optimal control method can improve the transient response performance of the current controller in the saturated state. When the system returns to the steady state, the algorithm automatically returns to the maximum torque current ratio control. This control method not only meets the improvement of the transient performance of the system, but also ensures the maximum torque control in the steady state. For most flux weakening control methods [31,32], the main concern is that the system can achieve high speed steady-state situation, that is, when the output voltage reaches the bus voltage saturation value, in order to achieve stable current control above the base speed, it is necessary to weaken the stator flux linkage, that is, using the excitation current component in the stator side to achieve demagnetization. It sacrifices torque performance in exchange for high speed.

2. Design of Current Time Optimal Controller

Due to the inherent characteristics of the PI regulator, the method of simply compensating the delay error of the digital system cannot further improve the dynamic performance of the current loop. To achieve real-time and rapid torque adjustment, it is necessary to control both the excitation current and the torque current in the transient process. On the basis of current delay error compensation, the high dynamic performance of PMSM under high speed condition is further improved by improving the time optimal current control method.

The state equation of PMSM in $\alpha\beta$ static coordinate system is

$$\begin{cases} \dfrac{di_\alpha}{dt} = \dfrac{-Ri_\alpha - e_\alpha + u_\alpha}{L} \\ \dfrac{di_\beta}{dt} = \dfrac{-Ri_\beta - e_\beta + u_\beta}{L} \end{cases} \tag{1}$$

where u_α and u_β are $\alpha\beta$ axis voltage respectively, i_α and i_β are $\alpha\beta$ axis current respectively, R and L are stator resistance and inductance respectively, e_α and e_β are $\alpha\beta$ axis back EMF respectively, and $e_\alpha = -\omega_e \psi_f \sin\theta_e$, $e_\beta = \omega_e \psi_f \cos\theta_e$, θ_e is rotor electrical angle, ω_e is rotor electrical angular velocity, ψ_f is rotor flux linkage.

Assuming that E_d and E_q are back EMF in dq rotating coordinate system, the back EMF in $\alpha\beta$ static coordinate system after $t = 0$ can be expressed as

$$\begin{cases} e_\alpha = E_d \cos\theta_e - E_q \sin\theta_e \\ e_\beta = E_d \sin\theta_e + E_q \cos\theta_e \\ \theta_e = \omega_e t + \theta_{e0} \end{cases} \tag{2}$$

The back EMF in dq rotating coordinate system (E_d, E_q) are closely related to the motor speed and magnetic flux ($E_d = 0$, $E_q = \omega_e \psi_f$), and they change slowly in a short time. Therefore, in most cases, the back EMF in dq rotating coordinate system can be assumed to be constant in a short time.

By introducing equation (2) into equation (1), the equation of state is rewritten as

ISSN: 2414-1895 DOI: 10.6919/ICJE.202507_11(7).0018

$$\begin{cases} \dfrac{di_\alpha}{dt} = \dfrac{-Ri_\alpha - E_d \cos\theta_e + E_q \sin\theta_e + u_\alpha}{L} \\ \dfrac{di_\beta}{dt} = \dfrac{-Ri_\beta - E_d \sin\theta_e - E_q \cos\theta_e + u_\beta}{L} \end{cases} \tag{3}$$

The initial state $t = 0$ of the system is

$$\begin{cases} i_\alpha(0) = i_{\alpha 0} \\ i_\beta(0) = i_{\beta 0} \end{cases} \tag{4}$$

The target state ($t = t_f$) is

$$\begin{cases} i_\alpha(t_f) = i_\alpha^* \\ i_\beta(t_f) = i_\beta^* \end{cases} \tag{5}$$

The control constraints are

$$\begin{cases} |u(t)| \le u_{\max} \\ 0 \le t \le t_f \end{cases} \tag{6}$$

The performance index is

$$J = \int_0^{t_f} dt = t_f \tag{7}$$

where $i_{\alpha 0}, i_{\beta 0}$ are the initial currents of $\alpha\beta$ axis at $t = 0$. i_α^*, i_β^* are the reference currents of $\alpha\beta$ axis at $t = t_f$. $u(t)$ is the system control input (u_α, u_β), and $u_{\max}$ is the maximum value of control input. t_f is the performance index, that is, the time taken for the system to reach the target value.

Now, the problem of the current control is to determine the control voltages which will force the currents to the reference current in the minimum possible time.

According to the above system description, the Hamiltonian function H for this problem is as follows:

$$H = 1 + (-Ri_\alpha - E_d \cos\theta_e + E_q \sin\theta_e + u_\alpha)\frac{p_\alpha}{L} + (-Ri_\beta - E_d \sin\theta_e - E_q \cos\theta_e + u_\beta)\frac{p_\beta}{L} \tag{8}$$

where p_α and p_β are the costate variables.

Because the control variable is bounded and the condition of $\partial H / \partial x = 0$ is not tenable, the conventional method can not solve the maximum or minimum value of the equation. Therefore, according to Pontryagin's minimum principle, the optimal control problem of continuous system under this condition is solved, that is, H function global minimum is used to replace the coupling

ISSN: 2414-1895 DOI: 10.6919/ICJE.202507_11(7).0018

equation. From the form of coupling equation, it can be understood as the maximum or minimum condition of solving H function. The Hamiltonian function H is solved by using the minimum principle.

The costate variables are the solution of the differential equations, such as

$$\begin{cases} \dfrac{dp_\alpha}{dt} = -\dfrac{\partial H}{di_\alpha} = \dfrac{R}{L} p_\alpha \\ \dfrac{dp_\beta}{dt} = -\dfrac{\partial H}{di_\beta} = \dfrac{R}{L} p_\beta \end{cases} \tag{9}$$

Solve the differential equation, and then the costate variables are given by

$$\begin{cases} p_\alpha = a_\alpha e^{(R/L)t} \\ p_\beta = a_\beta e^{(R/L)t} \end{cases} \tag{10}$$

where a_α and a_β are constant.

The value of p_α and p_β can be solved to obtain the control input $u(t)$ to minimize the function globally. Given such a control input, the current transient transition time can be minimized.

From the above derivation, it can be seen that the realization of optimal control is related to the initial state, the target state and the state with bounded control input. Under different control input limits, the control process and results are different. When designing the current controller, the output voltage should not only be amplitude limited, but also the voltage active area should be smaller than the SVPWM limit circle voltage range. The voltage constraints are shown in Figure 1. In the figure, u_d and u_q are dq axis actual voltage, u_d^* and u_q^* are dq axis regulator output voltage, and u_{dreal}^* and u_{qreal}^* are dq axis regulator output voltage after limited amplitude. U_{dc} is DC bus Voltage.

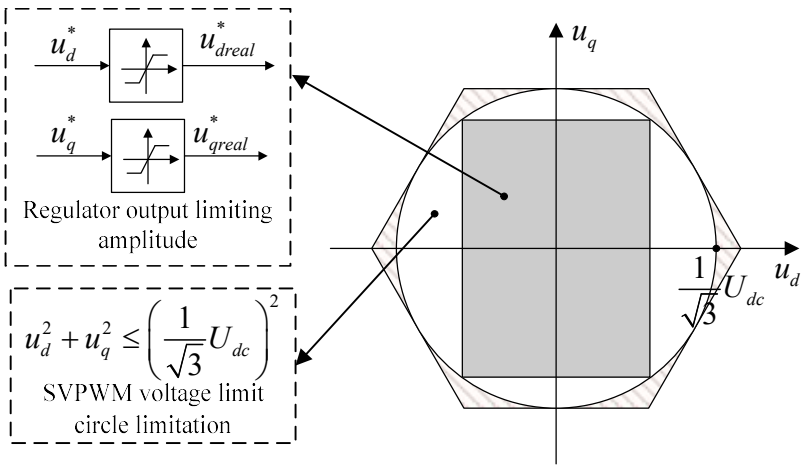

Figure 1. Voltage constraints

In the following, the current time optimal controller is designed according to the different voltage control input limits.

ISSN: 2414-1895 DOI: 10.6919/ICJE.202507_11(7).0018

2.1 Design of Current Time Optimal Control Algorithm under SVPWM Voltage Limit Circle Limitation

When the current regulator has no output limiting, the maximum output voltage of the inverter is limited by the bus voltage and SVPWM modulation mode, that is, the maximum output voltage of the inverter is limited by the voltage limit circle. Therefore, the bounded conditions of voltage control input are as follows:

$$(u_\alpha^2 + u_\beta^2) = (u_d^2 + u_q^2) \le (\frac{1}{\sqrt{3}} U_{dc})^2 = u_{\max}^2 \tag{11}$$

Combined with equation (9) and equation (11), according to Pontryagin's minimum principle, the values of control voltages (u_α ,u_β) are as follows in order to minimize the Hamiltonian function H :

$$\begin{cases} u_\alpha = u_{\max} \dfrac{p_\alpha}{\sqrt{p_\alpha^2 + p_\beta^2}} \\ u_\beta = u_{\max} \dfrac{p_\beta}{\sqrt{p_\alpha^2 + p_\beta^2}} \end{cases} \tag{12}$$

By introducing equation (10) into equation (12), the control voltage changes as follows:

$$\begin{cases} u_\alpha = u_{\max} \dfrac{a_\alpha}{\sqrt{a_\alpha^2 + a_\beta^2}} \\ u_\beta = u_{\max} \dfrac{a_\beta}{\sqrt{a_\alpha^2 + a_\beta^2}} \end{cases} \tag{13}$$

According to equation (13), since a_α and a_β are constant, the control voltages (u_α ,u_β) turn out to be constant.

By solving (3), the states (i_α , i_β) are given by the following equations:

$$\begin{cases} i_\alpha = (1 - e^{-(R/L)t}) \dfrac{u_\alpha}{R} + (K_2 \cos\theta_{e0} - K_1 \sin\theta_{e0} + i_{\alpha 0}) e^{-(R/L)t} - K_2 \cos\theta_e + K_1 \sin\theta_e \\ i_\beta = (1 - e^{-(R/L)t}) \dfrac{u_\beta}{R} + (K_1 \cos\theta_{e0} + K_2 \sin\theta_{e0} + i_{\beta 0})\, e^{-(R/L)t} - K_1 \cos\theta_e - K_2 \sin\theta_e \end{cases} \tag{14}$$

Where

ISSN: 2414-1895 DOI: 10.6919/ICJE.202507_11(7).0018

$$\begin{cases} K_1 = \dfrac{RE_q - (\omega_e L)E_d}{R^2 + (\omega_e L)^2} = \dfrac{R\omega_e \psi_f}{R^2 + (\omega_e L)^2} \\ K_2 = \dfrac{RE_d - (\omega_e L)E_q}{R^2 + (\omega_e L)^2} = \dfrac{\omega_e^2 L\psi_f}{R^2 + (\omega_e L)^2} \end{cases} \tag{15}$$

Let t_f^* be the minimum time required to force the initial states($i_{\alpha 0}, i_{\beta 0}$) to the reference states ($i_\alpha(t_f^*)$, $i_\beta(t_f^*)$). The reference currents are given by the following equations:

$$\begin{cases} i_\alpha(t_f^*) = i_d^* \cos\theta_e^* - i_q^* \sin\theta_e^* \\ i_\beta(t_f^*) = i_d^* \sin\theta_e^* + i_q^* \cos\theta_e^* \end{cases} \tag{16}$$

where θ_e^* is defined as

$$\theta_e^* = \omega_e t_f^* + \theta_{e0} \tag{17}$$

By introducing equation (16) into equation (14), the control voltages can be determined

$$\begin{cases} u_\alpha^* = \dfrac{R}{1 - e^{-(R/L)t_f^*}} \left\{ -(K_2 \cos\theta_{e0} - K_1 \sin\theta_{e0} + i_{\alpha 0}) e^{-(R/L)t_f^*} + (K_2 + i_d^*)\cos\theta_e^* - (K_1 + i_q^*)\sin\theta_e^* \right. \\ u_\beta^* = \dfrac{R}{1 - e^{-(R/L)t_f^*}} \left\{ -(K_1 \cos\theta_{e0} + K_2 \sin\theta_{e0} + i_{\beta 0}) e^{-(R/L)t_f^*} + (K_1 + i_q^*)\cos\theta_e^* + (K_2 + i_d^*)\sin\theta_e^* \right. \end{cases} \tag{18}$$

where u_α^* and u_β^* are given control voltages of $\alpha\beta$ axis.

2.2 Design of Current Time Optimal Control Algorithm under Regulator Output Voltage Limiting Amplitude

When the current regulator output is amplitude limited, the control voltage can be expressed as

$$\begin{cases} |u_\alpha| \le k_a U_{\max} \\ |u_\beta| \le k_\beta U_{\max} \end{cases} \tag{19}$$

where $U_{\max} = (1/\sqrt{3})U_{dc}$, k_α and k_β are constant, and $k_\alpha^2 + k_\beta^2 = 1$.

Under the above voltage constraints, according to Pontryagin's minimum principle, the values of control voltage input is as follows to minimize the Hamilton function H

$$u^*(t) = kU_{\max} sign(p(t)) = \begin{cases} +kU_{\max}, (p(t) > 0) \\ -kU_{\max}, (p(t) < 0) \end{cases} \tag{20}$$

ISSN: 2414-1895 DOI: 10.6919/ICJE.202507_11(7).0018

where $u^*(t)$ is the control voltage input under the above voltage constraints, $p(t)$ is the control voltage input without amplitude limited, and k is constant.

It can be seen from equation (20) that when the control input boundary is fixed, each component of the control vector should always take its own boundary value, thus forming the on-off control. For the current regulator, the output voltage command (u_α , u_β) always switches between $-k_\alpha U_{\max}(-k_\beta U_{\max})$ and $+k_\alpha U_{\max}(+k_\beta U_{\max})$. Combined with equation (10), the optimal phase trajectory and switch line of control voltages $(u_\alpha^*(t), u_\beta^*(t))$ can be drawn, as shown in Figure 2.

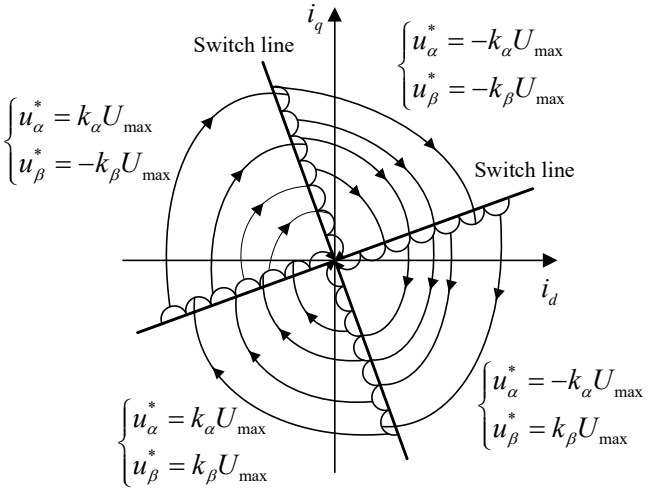

Figure 2. Optimal phase trajectory and switch line of control voltages

At this time, the control voltages are fixed value which is switched once every quarter cycle. Compared with the time optimal control under the condition of voltage limit circle, it can be seen that the complexity of current time optimal control is greatly affected by different voltage limiting conditions.

The derivation of the time optimal control algorithm under different voltage constraints shows that the control method is suitable for transient process. To design a complete current loop controller, it is necessary to add a steady state controller design. Let ρ be the definition of transient process, then the definition of transient process is as follows:

$$\sqrt{(i_d^* - i_d)^2 + (i_q^* - i_q)^2} > \rho \tag{21}$$

When the distance between the command current vector and the actual current vector is greater than a fixed value ρ, then the time is still in the transient process. From the definition of the transient process, it can be seen that the transient process is related to the dq axis current.

To sum up, the system block diagram of current time optimal controller for PMSM is shown in Figure 3. In the figure, i_a , i_b , i_c three-phase current, P is the number of pole pairs.

ISSN: 2414-1895 DOI: 10.6919/ICJE.202507_11(7).0018

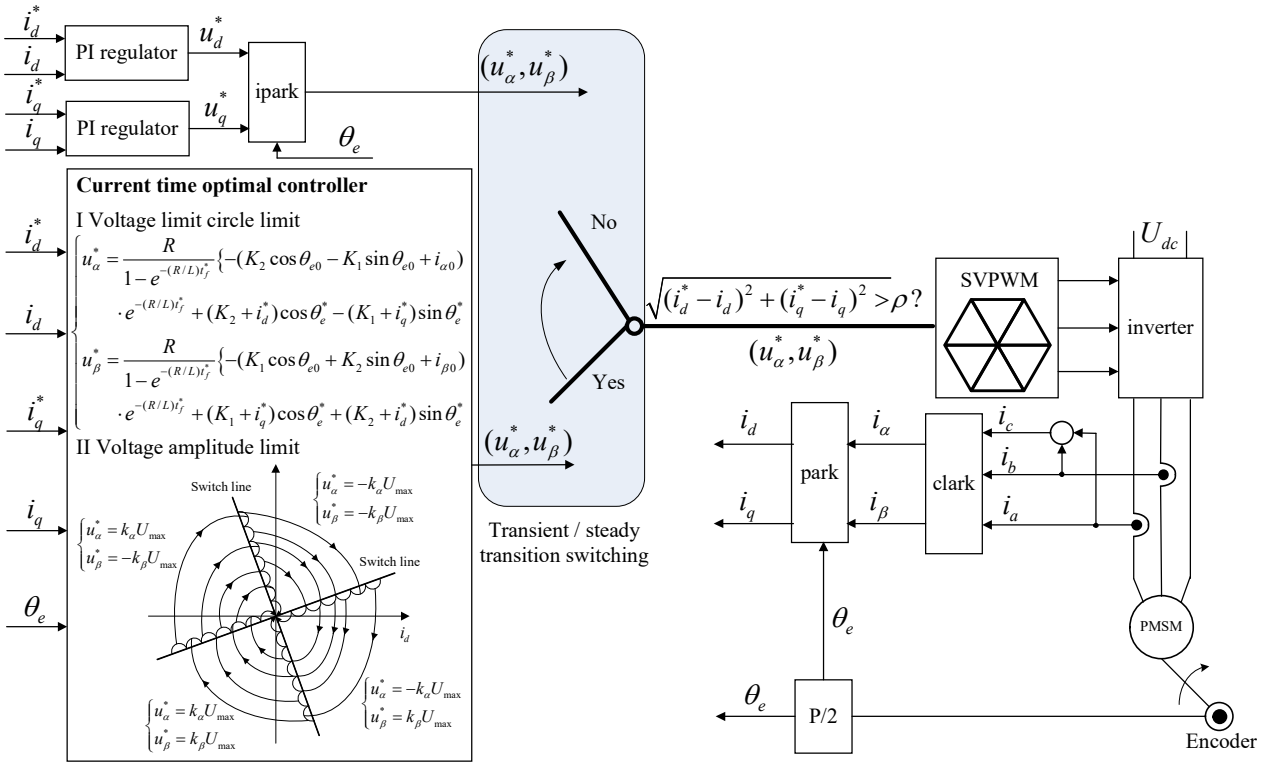

Figure 3. System block diagram of current time optimal controller for PMSM

3. Design of Improved Current Time Optimal Controller with Current Trajectory Planning

The improved time optimal control method is designed based on PI control. In order to improve the transient response, the PI regulator also realizes the anti saturation function. The structure block diagram of dq axis PI regulator is shown in Figure 4.

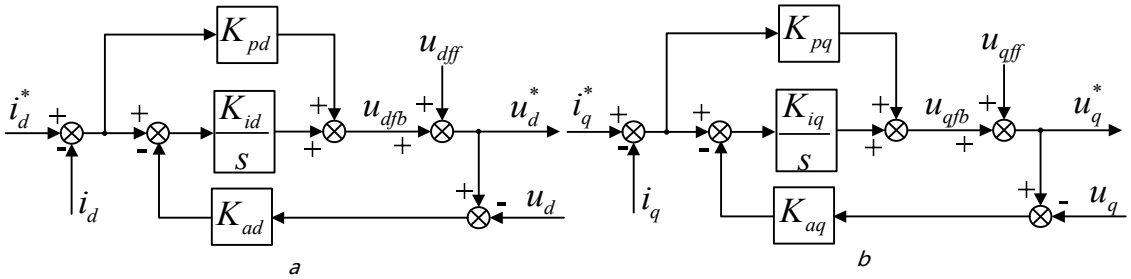

Figure 4. Structure block diagram of dq axis PI regulator

(a) PI regulator of d axis, (b) PI regulator of q axis

In the figure, u_d and u_q are the voltages after applying the circle limit or the amplitude limit. u_{dfb} and u_{qfb} are feedback voltages, and the expression are

$$\begin{cases} u_{dfb} = \dfrac{sK_{pd} + K_{id}}{s}\Delta i_d - \dfrac{K_{ad}K_{id}}{s}\Delta u_d \\ u_{qfb} = \dfrac{sK_{pq} + K_{iq}}{s}\Delta i_q - \dfrac{K_{aq}K_{iq}}{s}\Delta u_q \end{cases} \tag{22}$$

ISSN: 2414-1895 DOI: 10.6919/ICJE.202507_11(7).0018

where K_{pd} and K_{pq} are PI regulator proportional gains. K_{id} and K_{iq} are PI regulator integral gains. K_{ad} and K_{aq} are PI regulator anti saturation proportional gains. Δi_d and Δi_q are current error. Δu_d and Δu_q are voltage error, and the expression are

$$\begin{cases} \Delta i_d = i_d^* - i_d \\ \Delta i_q = i_q^* - i_q \\ \Delta u_d = u_d^* - u_d \\ \Delta u_q = u_q^* - u_q \end{cases} \tag{23}$$

u_{dff} and u_{qff} are feedforward voltages, which include back EMF and cross coupling part. The expression are

$$\begin{cases} u_{dff} = -\omega_e L i_q \\ u_{qff} = \omega_e (L i_d + \psi_f) \end{cases} \tag{24}$$

The output voltages of PI regulator (u_d^*, u_q^*) consist of feedforward voltage and feedback voltage. The expression are

$$\begin{cases} u_d^* = u_{dfb} + u_{dff} \\ u_q^* = u_{qfb} + u_{qff} \end{cases} \tag{25}$$

In order to make the transfer function of current loop as simple as possible, the zero pole cancellation method is used to make $\frac{K_{pd}}{K_{id}} = \frac{K_{pq}}{K_{iq}} = \frac{L}{R}$. Make ω_{bw} the cut-off frequency, usually 1/10 of the PWM frequency (10kHz), that is 1000Hz. The gain parameters design of PI controller is shown in Table 1.

Table 1. Parameters design of current loop PI controller

K_{pd}	K_{id}	K_{ad}	K_{pq}	K_{iq}	K_{aq}
$L\omega_{bw}$	$R\omega_{bw}$	$\frac{1}{K_{pd}}$	$L\omega_{bw}$	$R\omega_{bw}$	$\frac{1}{K_{pq}}$

When the bus voltage is fixed and the motor is in high speed state, the motor back EMF is large and the dynamic voltage margin of q axis is small , the output of current regulator at high speed will inevitably exceed the voltage saturation value. Take voltage limit circle for saturation condition, according to the over modulation control strategy of SVPWM, the voltage after over modulation will stay within the voltage limit circle. When the command voltage exceeds the voltage limit, the defect of poor dynamic performance of q axis current caused by small voltage margin is more obvious, and even the real q axis current can not track the command current. By making the d axis current in the

ISSN: 2414-1895 DOI: 10.6919/ICJE.202507_11(7).0018

transient process at a negative value, the voltage margin of the q axis increases, thus improving the dynamic performance of the q axis current.

Through the replanning of d axis transient command current trajectory, the replanned command current i_{dm}^* can be expressed as

$$i_{dm}^* = i_d^* - \frac{1}{K_{pd}}\Delta u_q \tag{26}$$

When $|K_{id}| \ll |sK_{pd}|$, the output d axis control voltage of the replanned d axis current command after passing through the PI current regulator can be expressed as

$$u_{d2}^* = u_{d1}^* - \frac{sK_{pd} + K_{id}}{s}\frac{\Delta u_q}{K_{pd}} \approx u_{d1}^* - \Delta u_q \tag{27}$$

where u_{d1}^* is the output control voltage of d axis before replanning d axis current, and u_{d2}^* is the output control voltage of d axis after replanning d axis current. Through the above process, the value of d axis output control voltage in the transient process is modified, and the negative direction of d axis current is increased finally.

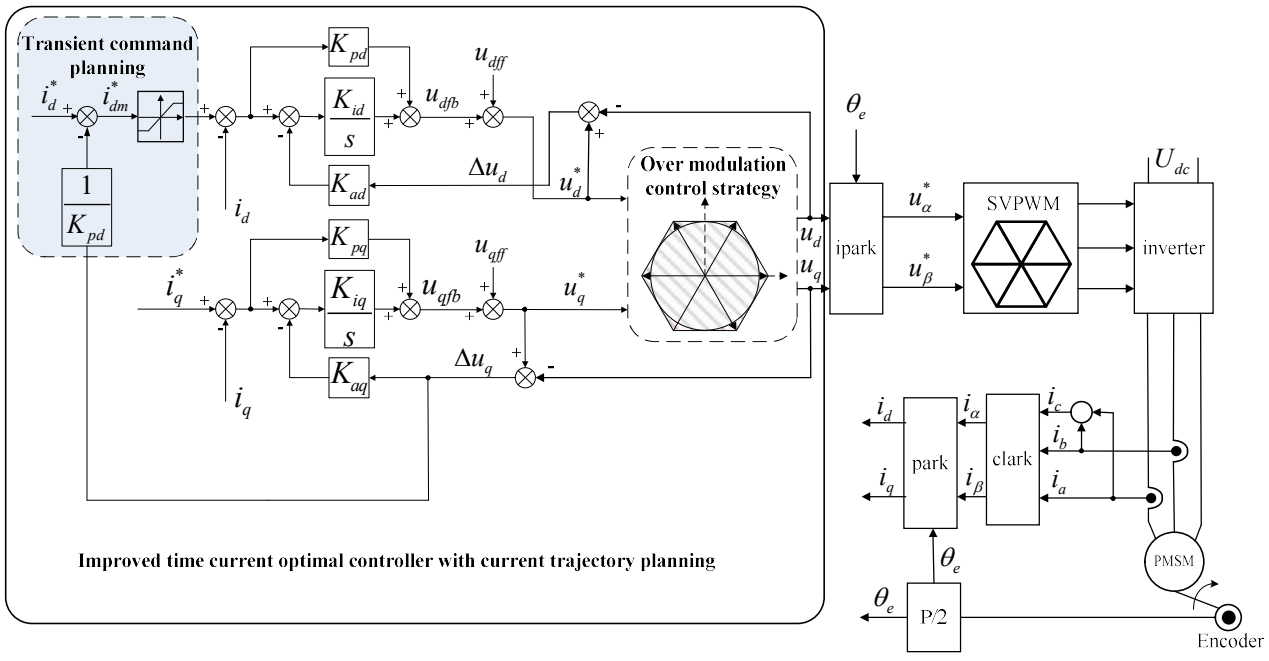

Figure 5. System block diagram of improved time current optimal controller with current trajectory planning for PMSM

According to equations (26) and (27), when the motor is running at high speed, the action steps of voltage command correction when the step current command occurs can be described as follows: after the q axis step command is given, the output voltage command u_q^* will be increased instantaneously to exceed the voltage limit circle after passing through the current controller. According to equation (27), under the premise of replanning the d axis current command to equation

ISSN: 2414-1895 DOI: 10.6919/ICJE.202507_11(7).0018

(26), the system can directly compensate the part of q axis voltage component exceeding the limit circle to the d axis voltage component, and the d axis output voltage value in the transient process is corrected, then finally the d axis current increases in a negative direction. To sum up, the system block diagram of improved time current optimal controller with current trajectory planning for PMSM is shown in Figure 5.

4. Experiment Results

To validate the effectiveness of the proposed current control method, experimental tests were carried out on a 2.2 kW PMSM test bench. Motor parameters are listed in Table 2. The double motor tow loading mode is used to provide load torque through a coaxially connected load motor (running in constant torque control mode). In the experimental tests, the developed algorithm is implemented on a 32-bit floating point DSP TMS320F28377, and the PWM frequency and current sampling frequency are given 10kHz.

Table 2. Motor parameters

Parameters	Units	Values
Rated power	kW	2.2
Rated voltage	V	220
Rated speed	rpm	4500
Rated torque	N.m	4.7
Rated current	A	10.5
Stator resistance	Ω	0.89
Inductance of dq axis	mH	2.5
Number of pole pairs		4
EMF constant	V/krpm	15

4.1 Current Time Optimal Controller

Under the no load condition of 4000rpm, the current transient response performance of the current time optimal control and the conventional PI control are compared by giving the step signal of 9A of the q axis current command. The system block diagram of current time optimal controller is shown in Figure 3. Figure 6 shows the comparison of transient response of dq axis current at 4000rpm. Among them, Figure 6(a) shows the waveform of time optimal control under voltage limit circle, Figure 6(b) shows the waveform of time optimal control under voltage limiting amplitude, and Figure 6(c) shows the waveform of conventional PI control. Time delay error compensation has been carried out for the above three control methods. Compared with Figure 6(a) and Figure 6(c), it can be seen that under higher speed condition, the time for optimal time control to reach the command current is about 3.3ms, while the response time of conventional PI control is about 4.7 ms, and the transient transition time is increased by about 29%. The voltage limit amplitude in Figure 6(b) is $k_\alpha = k_\beta = 1/\sqrt{2}$. Compared with Figure 6(b) and Figure 6(c), the current response time of the regulator under the condition of output voltage limiting amplitude is about 3.8ms, which is about 19% higher than that of the conventional PI controller. However, compared with the time optimal control under limit circle, it has obvious shortcomings. The analysis shows that the voltage operating region under the current regulator output voltage limiting condition is obviously smaller than that under the limit circle limit, and the dynamic performance of current is directly related to the voltage applied to RL load. At this time, the dynamic response is slightly worse than the current time optimal control under the limit circle limit condition. It can be seen from the current trajectories in Figure 6(a) and Figure 6(b) that

ISSN: 2414-1895 DOI: 10.6919/ICJE.202507_11(7).0018

the current trajectory with the shortest transient process time is not the current trajectory with $i_d = 0$, on the contrary, the d axis current is in the weak magnetic state.

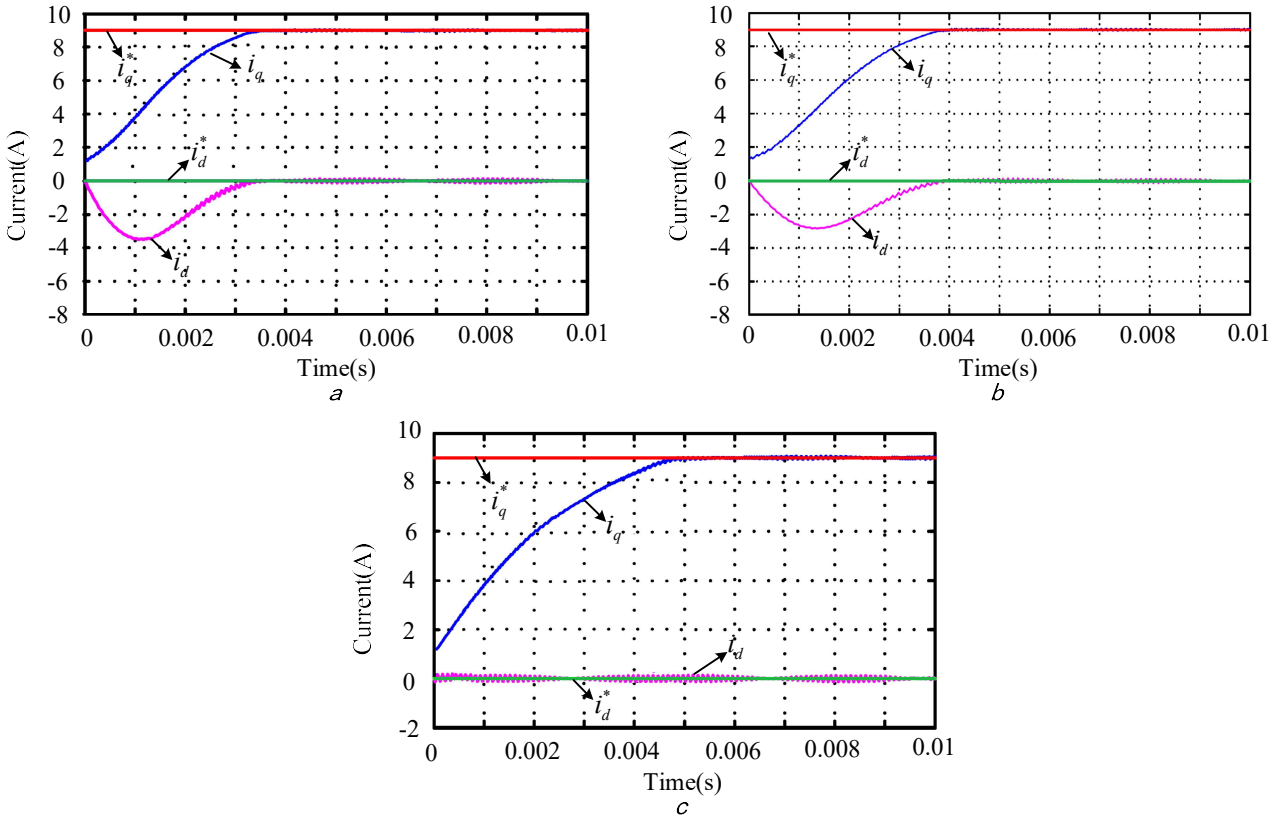

Figure 6. Comparison of transient response of dq axis current at high speed (Time optimal control) (a) Time optimal control under voltage limit circle, (b) Time optimal control under voltage limiting amplitude, (c) Conventional PI control

4.2 Improved Current Time Optimal Controller with Current Trajectory Planning

Similarly, under the no load condition of 4000rpm, the current transient response performance of the conventional PI control and the improved current time optimal control are compared by giving the step signal of 9A of the q axis current command. The system block diagram of improved current time optimal controller is shown in Figure 5, and the actual gain values of Figure 5 are: $K_{pd} = K_{pq} = 2500$, $K_{id} = K_{iq} = 890$, $K_{ad} = 1/K_{pd}$, $K_{aq} = 1/K_{pq}$. Figure 7 shows the comparison of transient response of dq axis current at 4000rpm. Among them, Figure 7(a) shows the waveform of conventional PI control, Figure 7(b) shows the waveform of improved current time optimal control with current trajectory planning. Time delay error compensation has been carried out for the above two control methods. Compared with Figure 7(a) and Figure 7(b), under the same condition, the transient transition time of improved time optimal control is about 3.4ms, and its transient transition time is about 27% higher than that of conventional PI controller. The trend of dq axis current trajectory in transient process is the same as that in Figure 6(a) when time optimal control is adopted. The above experiments show that the voltage command can be changed by d axis current command trajectory planning in the transient process, and the transient transition time of current can be shortened finally. It can be seen from Figure 7(b) that the d axis current command i_d^* is still 0 after the transient process, which can not only improve the transient performance, but also realize the steady state maximum torque control. Compared with Figure 6(a) and Figure 7(b), the transient transition time of improved time optimal control is almost the same as that of time optimal control. Compared with the conventional PI controller, the improved time optimal controller with current trajectory planning can improve the

ISSN: 2414-1895 DOI: 10.6919/ICJE.202507_11(7).0018

dynamic performance of torque output at high speed. Because the controller is simple and reliable, it can completely replace the current time optimal controller.

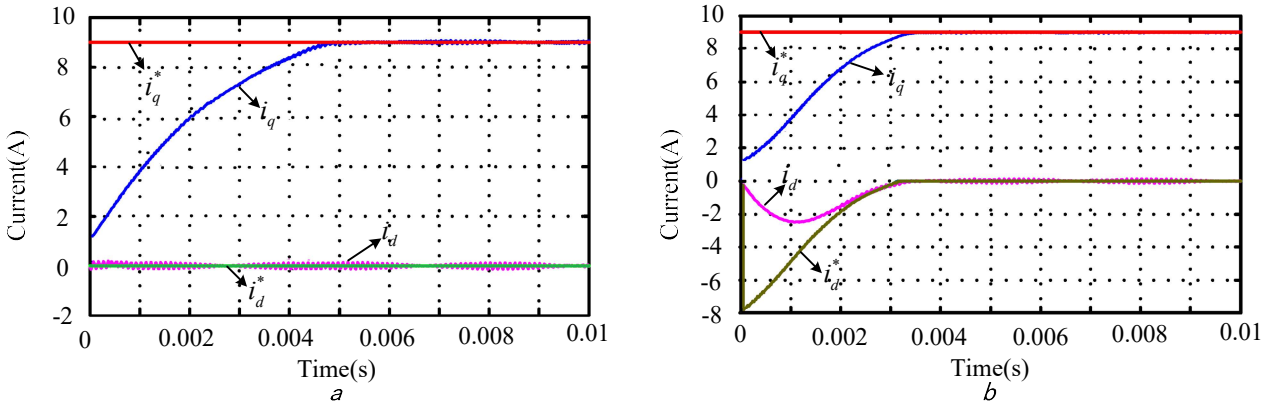

Figure 7. Comparison of transient response of dq axis current at high speed (Improved current time optimal control with current trajectory planning

(a) Conventional PI control, (b) Improved current time optimal control with current trajectory planning

5. Conclusion

This paper has presented a current time optimal control method to plan the voltage command to achieve the shortest current tracking time. Considering the computational complexity of the optimal control algorithm, an improved current time optimal control method is proposed by analyzing the time optimal current trajectory. The current transient transition trajectory is optimized by replanning the current command. The control method not only simplifies the calculation of the algorithm, but also realizes the fast transient-current characteristics in voltage saturation region without affecting the current steady state performance. The experimental results verify the advantages of the new current control method in maintaining system stability and fast transient current response at high speed.

Acknowledgments

The authors thank the editor and anonymous reviewers for their valuable remarks and helpful suggestions. This study was partially supported by the Provincial Research Platform Opening Fund of Yancheng Polytechnic College (YGKF2305).

References

[1] Wang Q., Zhang G., Wang G., et al.: ‘Offline Parameter Self-Learning Method for General-Purpose PMSM Drives With Estimation Error Compensation’, IEEE Trans. Power. Electron, 2019, 34, pp. 11103–11115

[2] Rafaq M S., Jung J W.: ‘A Comprehensive Review of State-of-the-Art Parameter Estimation Techniques for Permanent Magnet Synchronous Motors in Wide Speed Range’, IEEE Trans. Ind. Informatics, 2020, 16, pp. 4747–4758

[3] Ren J., Ye Y., Xu G., et al.: ‘Uncertainty-and-Disturbance-Estimator-Based Current Control Scheme for PMSM Drives With a Simple Parameter Tuning Algorithm’, IEEE Trans. Power. Electron, 2017, 32, pp. 5712–5722

[4] Toloue S F., Kamali S H., Moallem M.: ‘Multivariable Sliding-Mode Extremum Seeking PI Tuning for Current Control of A PMSM’, IET Electric Power Appl, 2020, 14, pp. 348–356

[5] Kim J., Seiya K., Edahiro M., Doki S.: ‘Analysis and Evaluation of Current Control System of PMSM with Time-Delay to Improve Parallelization for Implementation on Multi-Core Precessors’, 2019 22th

ISSN: 2414-1895 DOI: 10.6919/ICJE.202507_11(7).0018

International Conf. on Electrical Machines and Systems (ICEMS). Harbin, China, 2019, DOI: 10.1109/ICEMS.2019.8921506

[6] Lian C., Xiao F., Liu J., Gao S.: 'Analysis and Compensation of the Rotor Position Offset Error and Time Delay in Field-Oriented-Controlled PMSM Drives', IET Power Electric, 2020, 13, pp. 1911–1918

[7] Shang S., Yang M., Xu D., et al.: 'Enhanced Bandwidth of Current Loop for Permanent Magnet Synchronous Motor Drives Based on FPGA', 2018 21th International Conf. on Electrical Machines and Systems (ICEMS). Harbin, China, 2018, DOI: 10.23919/ICEMS.2018.8549304

[8] Wang H., Yang M., Niu L., Xu D.: 'Current-Loop Bandwidth Expansion Strategy for Permanent Magnet Synchronous Motor Drives', 2010 5th IEEE Conf. on Industrial Electronics and Applications. Taichung, Taiwan, 2010, DOI: 10.1109/ICIEA.2010.5514913

[9] Liu J., Li H., Deng Y.: 'Torque Ripple Minimization of PMSM Based on Robust ILC Via Adaptive Sliding Mode Control', IEEE Trans. Power. Electron, 2018, 33, pp. 3655–3671

[10] Mani P., Rajan R., Shanmugam L., Joo Y H.: 'Adaptive Fractional Fuzzy Integral Sliding Mode Control for PMSM Model', IEEE Trans. Fuzzy. Systems, 2019, 27, pp. 1674–1686

[11] Zhao Y., Liu X., Yu H., Yu J.: 'Model-Free Adaptive Discrete-Time Integral Terminal Sliding Mode Control for PMSM Drive System with Disturbance Observer', IET Electric Power Appl, 2020, 14, pp. 1756–1765

[12] Toloue S F., Kamali S H., Moallem M.: 'Multivariable Sliding-Mode Extremum Seeking PI Tuning for Current Control of a PMSM', IET Electric Power Appl, 2020, 14, pp. 348–356

[13] Jung J W., Choi Y S., Leu V Q., Choi H H.: 'Fuzzy PI-Type Current Controllers for Permanent Magnet Synchronous Motors', IET Electric Power Appl, 2011, 5, pp. 143–152

[14] Victor M., Hernandez G., Ramon S O.: 'PI Control Plus Electric Current Loops for PM Synchronous Motors', IEEE Trans. Control Systems Technology, 2011, 19, pp. 868–873

[15] Khiabani A G., Heydari A.: 'Optimal Torque Control of Permanent Magnet Synchronous Motors Using Adaptive Dynamic Programming', IET Power Electric, 2020, 13, pp. 2442–2449

[16] Smidl V., Janous S., Peroutka Z., Adam L.: 'Time-Optimal Current Trajectory for Predictive Speed Control of PMSM Drive', 2017 IEEE International Symposium. on IPredictive Control of Electrical Drives and Power Electronics (PRECEDE). Pilsen, Czech Republic, 2010, DOI: 10.1109/PRECEDE.2017.8071273

[17] Aghili F.: 'Optimal Feedback Linearization Control of Interior PM Synchronous Motors Subject to Time-Varying Operation Conditions Minimizing Power Loss', IEEE Trans. Ind. Electron, 2018, 65, pp. 5414–5421

[18] Gao J., Gong C., Li W., Liu J.: 'Novel Compensation Strategy for Calculation Delay of Finite Control Set Model Predictive Current Control in PMSM', IEEE Trans. Ind. Electron, 2020, 67, pp. 5816–5819

[19] Siami M., Khaburi D A., Rivera M., Rodriguez J.: 'An Experimental Evaluation of Predictive Current Control and Predictive Torque Control for a PMSM Fed by a Matrix Converter', IEEE Trans. Ind. Electron, 2017, 64, pp. 8459–8471

[20] Zhang Y., Huang L., Xu D., et al.: 'Performance evaluation of two-vector-based model predictive current control of PMSM drives', Chinese Journal of Electrical Engineering, 2018, 4, pp. 65–81

[21] Petkar S G., Kumar T V.: 'Computationally Efficient Model Predictive Control of Three-Level Open-End Winding Permanent-Magnet Synchronous Motor Drive', IET Electric Power Appl, 2020, 14, pp. 1210–1220

[22] Wu G., Huang S., Wu Q., et al.: 'Robust Predictive Torque Control of N*3-Phase PMSM for High-Power Traction Application', IEEE Trans. Power. Electron, 2020, 35, pp. 10799–10809

[23] Seok J K., Kim J S., Sul S K.: 'Overmodulation Strategy for High-Performance Torque Control', IEEE Trans. Power. Electron, 1998, 13, pp. 786–792

[24] Bae B H., Sul S K.: 'A Novel Dynamic Overmodulation Strategy for Fast Torque Control of High-Saliency-Ratio AC Motor', IEEE Trans. Ind. Appl, 2005, 41, pp. 1013–1019

[25] Lerdudomsak S., Kadota M., Doki S., Okuma S.: 'Novel Techniques for Fast Torque Response of IPMSM Based on Space-Vector Control Method in Voltage Saturation Region', IECON 2007 33rd Annual

ISSN: 2414-1895 DOI: 10.6919/ICJE.202507_11(7).0018

Conference of the IEEE Industrial Electronics Society. Taipei, Taiwan, 2007, DOI: 10.1109/IECON.2007.4459935

[26] Lerdudomsak S., Doki S., Okuma S.: 'Voltage Limiter Calculation Method for Fast Torque Response of IPMSM in Overmodulation Range', 2009 35th Annual Conf. on IEEE Industrial Electronics. Porto, Portugal, 2009, DOI: 10.1109/IECON.2009.5414701

[27] Choi J W., Sul S K.: 'Generalized Solution of Minimum Time Current Control in Three-Phase Balanced Systems', IEEE Trans. Ind. Electron, 1998, 45, pp. 738–744

[28] Bolognani S., Tomasini M., Tubiana L., Zigliotto M.: 'DSP-based time optimal current control for high dynamic IPM motor drives', 2004 35th Annual Power Electronics Specialists Conference. Aachen, Germany, 2004, DOI: 10.1109/PESC.2004.1355461

[29] Choi J W., Sul S K.: ' Design of Fast-Response Current Controller Using DQ Axis Cross Coupling: Application to Permanent Magnet Synchronous Motor Drive', IEEE Trans. Ind. Electron, 1998, 45, pp. 522–524

[30] Maric D S., Hiti S., Stancu C C., et al.: 'Two Flux Weakening Schemes for SurfaceMounted Permanent-Magnet Synchronous Drives. Design and Transient Response Considerations', ISIE '99. Proceedings of the IEEE International Symposium on Industrial Electronics. Bled, Slovenia, 1999, DOI: 10.1109/ISIE.1999.798693

[31] Evans D J., Zhu Z Q., Zhan H L., et al.: 'Flux-Weakening Control Performance of Partitioned Stator-Switched Flux PM Machines', IEEE Trans. Ind. Appl, 2016, 52, pp. 2350–2359

[32] Xu Y., Morito C., Robert D.: 'Extending High-Speed Operating Range of Induction Machine Drives Using Deadbeat-Direct Torque and Flux Control With Precise Flux Weakening', IEEE Trans. Ind. Appl, 2019, 55, pp. 3770–3780